Athens Journal of Technology and Engineering - Volume 10, Issue 3,
September 2023 – Pages 147-160

Quantifying Shallow-Depth Concrete Delamination using Impact-Echo

By Mantaka Mahjabin Momo[*]*, Nur Yazdani*[±] *& Eyosias Beneberu*[°]

Corrosion-induced concrete deck delamination is quite common in bridges. Locating these embedded delaminations is important to assess the extent of the damage, the remaining member capacity and any necessary rehabilitation. The impact-echo (IE) is a simple and straightforward non-destructive testing (NDT) technique by which the depth and extent of concrete delamination may be estimated. It is effective in detecting the location and determining the depth of relatively deep delaminations in concrete. Delaminations that occur near the concrete surface can also be detected by the IE method. However, the exact depth cannot be quantified due to difficulties in analysing the flexural mode that dominates the vibration response over the corresponding delaminated region. This study developed an IE-based procedure to quantitatively estimate the depth of shallow depth delaminations in concrete slab members. Four slab specimens were prepared, each with three artificial delaminations with varying shapes and sizes at shallow depths. The frequency contour maps showed good agreement with the actual location of the delaminations. The perimeter-to-depth ratio of the delaminated region can be used to analyze the flexural mode vibration frequency. Two equations are proposed that relate the depth of arbitrarily shaped delaminations to the flexural mode vibration frequency measured over the shallow-depth delaminations.

Keywords: *impact echo, concrete delamination, concrete slabs, flexural mode vibration, non-destructive evaluation (NDE)*

Introduction

Near-surface delaminations, a defect that may be commonly found in concrete slabs and bridge decks, play a significant role in decreasing structural integrity. They can form due to steel reinforcing bar corrosion. If they are not detected early in their formation stage, the defects may keep growing with time, resulting in the need for interventions in the form of costly large-scale repairs and retrofitting of the affected structures.

Non-destructive testing (NDT) methods can be being used successfully to detect damage within concrete structures, and several NDT methods in particular have shown potential for locating internal delaminations. In general, each NDT method is best suited for characterizing a specific type of deterioration (Gucunski et al. 2017). For example, ground penetrating radar (GPR) can detect corrosive

[*]Project Engineer, Stiver Engineering, Houston, TX, USA.
[±]Professor, University of Texas at Arlington, USA.
[°]Structural Engineer, BridgeFarmer, Inc., Dallas, TX, USA.

https://doi.org/10.30958/ajte.10-3-1 doi=10.30958/ajte.10-3-1

environment which indirectly implies the likelihood of delaminated region within the structure. Infrared thermography (IR) detects the subsurface defects by using temperature dependent electromagnetic radiation surface radiation (Kee et al. 2012). The Impact Echo (IE) is a mechanical wave-based NDT technique that has been widely and effectively used in identifying the location and extent of the delaminated regions (Kee et al. 2012, Gucunski et al. 2012, Zhu and Popovics 2007). In this method, a short duration impact is applied on the test surface and the subsequent vibration response is received by a transducer placed close to the point of impact. The transient stress pulse generated from the applied impact propagates through the structure as three stress waves, namely P-, S- and R-waves. The time domain signal acquired from the transducer can be converted into frequency domain by using fast Fourier transform (FFT). If the transducer is placed close to the impact point, the response is dominated by the P-wave (Carino 2001, Carino and Sansalone 1990, Cheng and Sansalone 1993a, Sansalone and Carino 1986). The peak frequency, f in the amplitude spectrum is related to the depth of reflecting interface and the P-wave velocity, $C_{p,}$ in accordance with the following equation:

$$f = \frac{0.96C_P}{2T} \tag{1}$$

where, T = the distance between the two reflecting surfaces (top surface and delamination)

Equation 1 is used to evaluate the IE test results and is based on the repetitive arrival of the P-wave as it undergoes multiple reflection between the two reflecting surfaces. This particular mode is the thickness mode frequency, but in the presence of shallow delamination, the flexural mode vibration of the delaminate portion of the plate dominates the frequency response. The depth up to which the IE flexural mode dominates the response is around 102 mm (12), and any depth smaller than this value is referred to as a shallow depth in this study. This vibration mode represents the out-of-plane movement of the section above the delaminated region and depends on several parameters, such as the material properties, boundary conditions and the geometry of the delaminated section (Kee and Gucunski 2016). Consequently, the IE-detected flexural mode of vibration cannot be interpreted by Equation 1.

In a previous study (Cheng and Sansalone 1993a), an analytical model, based on the flexural vibration of a simply supported thick plate, was proposed to estimate the vibration response of shallow depth delaminations. However, the model yielded erroneous results, because the boundaries for the delaminated section were more rigid than the assumed simply supported boundary condition. Another study found that the response above a shallow depth delamination lies between the simply supported and clamped boundary conditions of classical thin plate vibration (Oh et al. 2013b). In this study, the edge effect, with a correction function, was employed as a simple semi-analytical expression to relate the flexural mode of vibration to the geometry of delamination for a width-to-depth ratio greater than five. Another semi-analytical formulation was proposed, in

which the rectangular delaminated region was converted to an equivalent square shape with a width of "*c*", and the geometry of the delamination was correlated with the flexural mode vibration frequency (Kee and Gucunski 2016). This study suggested that the effect of the type of boundary condition increases as the width-to-depth ratio (*c/h*) decreases, and it is more prominent when this ratio is less than five. These previous studies considered only regularly-shaped (rectangular, square, or circular) delaminations, and the suggested analytical expressions were based on the length or width of the simulated delaminations. In practice, delaminations have arbitrary shapes and may not have any well-defined lengths or widths. It is apparent that the previous studies were limited in scope in terms of unsuitability for quantifying arbitrarily shaped shallow-depth delaminations. This severely limits the applicability of these existing models. The current study was undertaken to fill this important knowledge gap by developing an analytical expression that can interpret the IE-detected flexural vibration mode for arbitrarily-shaped delaminations and also estimate the depth of shallow-depth delaminations.

Test Specimens

Four reinforced concrete slabs with artificially created delaminations were prepared. The slabs were 150 mm thick and had dimensions of 1200 x 1200 mm. The thickness was chosen so that the artificial delaminations could be placed at shallow depths, as it has been reported that the IE flexural vibration response is excited only if the delamination is shallower than 100 mm (Impact-Echo User's Manual 2001). Each slab contained three artificial delaminations, as shown in Figure 1. The delaminations were simulated by acrylic sheets (of 2.36 mm thick) with specific shapes and sizes that were covered with two layers of plastic sheets, as shown in Figure 3. To facilitate the positioning of the delaminations, two layers of # 4 (12.7 mm) bars were placed along orthogonal directions, and the delaminations were placed on top of the reinforcing bars at depths of either 38 mm or 83 mm depth. Plan and cross section views of Slab 2 are presented in Figure 2. The delamination designations and corresponding depths, areas and perimeters are given in Table 1.

Figure 1. *Slab Plan Views with Delaminations Shaded in Black and Grid Used for Testing*

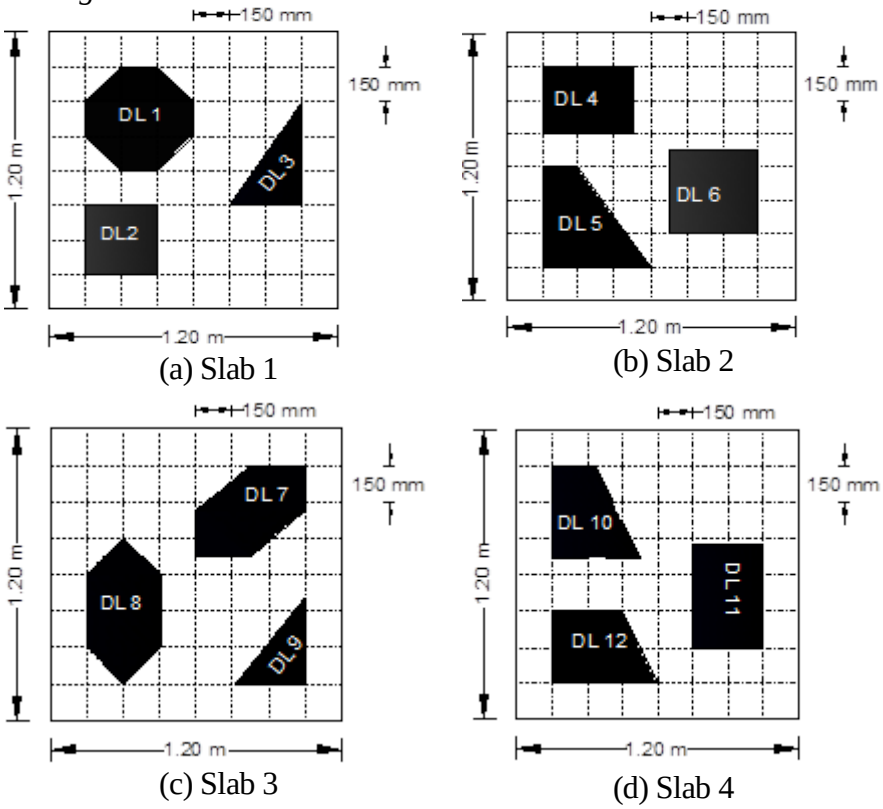

Figure 2. *Slab 2 Plan and Cross Section Views with Additional Details*

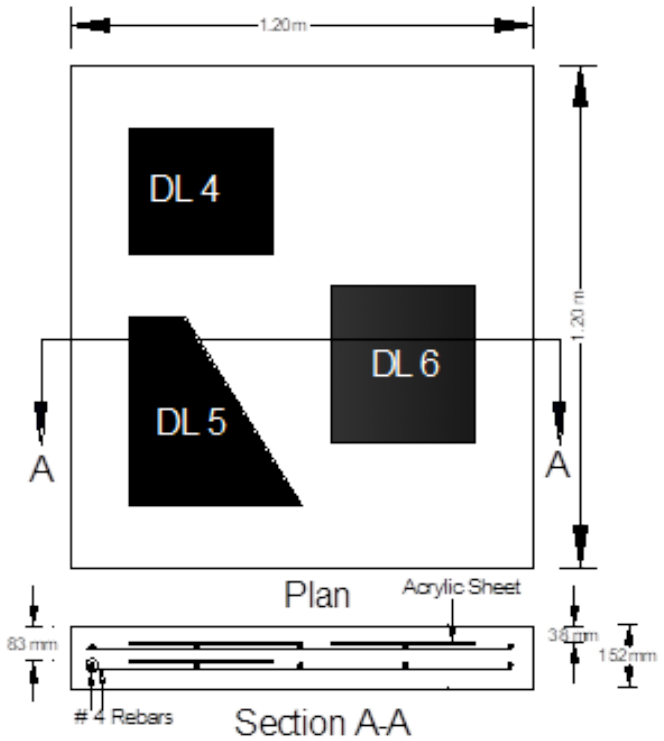

Figure 3. *Prefabricated Delamination Placement*

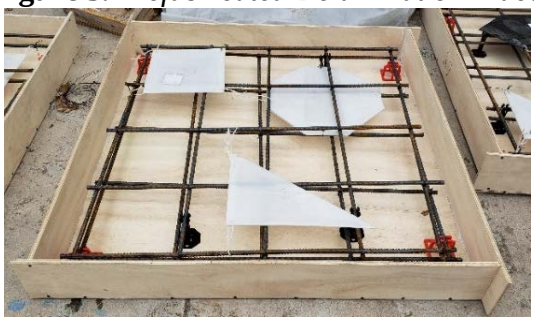

(a) Slab 1

(b) Slab 2

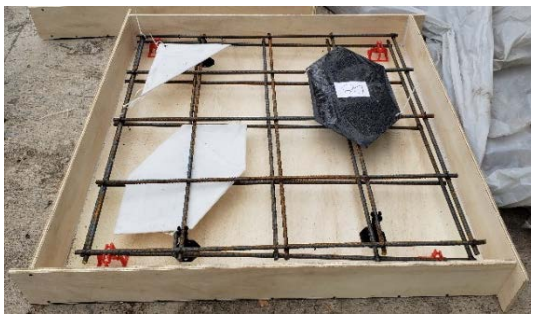

(c) Slab 3

(d) Slab 4

Table 1. *Detailed Information of the Prefabricated Delaminations*

Delamination No.	Shape	Area (m^2)	Perimeter (m)	Depth (mm)
DL1	Octagon	0.16	1.5	83
DL2	Rectangle	0.09	1.2	38
DL3	Triangle	0.07	1.3	38
DL4	Rectangle	0.12	1.4	83
DL5	Trapezoid	0.14	1.6	38
DL6	Rectangle	0.15	1.5	38
DL7	Hexagon	0.14	1.5	83
DL8	Hexagon	0.14	1.5	38
DL9	Triangle	0.06	1.1	38
DL10	Trapezoid	0.11	1.4	83
DL11	Rectangle	0.12	1.4	38
DL12	Trapezoid	0.11	1.4	38

Specimen Preparation

Typical concrete mixture proportions used for the test slabs is presented in Table 2. The target slump and com-pressive strength at 28 days were 200 mm and 20.7 MPa, respectively. The test slabs were cast from a single batch of ready-mix concrete from a local plant. Plywood formwork was used. After application of curing compound, the slabs were cured for 28 days. The concrete compressive strength was determined from the average of three cylindrical specimens (100 x 200 mm size), evaluated in accordance with ASTM C39/C39M (ASTM 2020) at 28 day age.

Table 2. *Concrete Mix Design*

Ingredient	**Amount (kg/m^3)**
Cement	201
Fly Ash	51
Water	141
Coarse aggregate	1098
Fine aggregate (Bristol sand)	214
Fine aggregate (Bridgeport sand)	640

NDE Procedure

We used a commercially available Impact Echo (IE) device with the following characteristics. It has an LCD backlit touch screen with a touchscreen keyboard for entering 5-character file names, depicted in Figure 4. For the signal input it has up to 4 wide band channels with 16 bit analog/digital converters. The equipment includes a test head with a solenoid impactor and built-in transducer as shown in Figure 5. The impactor applies force on the test surface, the corresponding vibration response is measured by the transducer, and the transducer response is analyzed and displayed on the display platform.

Figure 4. *Components of the IE System (Test Head, Cable, and Display Unit)*

Figure 5. *Components of the IE Test Head (Transducer and Solenoid Impactor)*

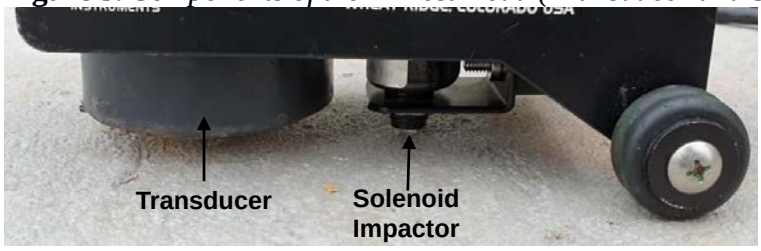

For the IE testing, a 150 x 150 mm grid pattern as shown in Figure 1. This grid size was selected so that there would be multiple test point over each delamination. Previous studies used both 300 x 300 mm and 150 x 150 mm grid spacings (Lee et al. 2017, Kee and Gucunski 2016). We used the smaller grid size as our specimens were relatively small.

For testing, the test head was firmly pressed at each grid point in sequence and the solenoid impactor was activated. The collected waveforms were stored and then post-processed. The P-wave velocity obtained from tests at solid locations was 3232 m/s, constant at each grid point. The peak frequency at each grid point was determined by using the WinIE software (Olson Instruments, Inc. 2016). In accordance with Equation 1, the thickness frequency at the solid portion is 10.3 kHz. Similarly, the thickness mode frequency for delaminations at 38mm will be 40.8 kHz and for the delaminations at 83mm this value will be 18.7 kHz.

Results and Discussion

The first step in the data analysis was to determine the frequency at each grid point. Frequency contour maps with zones of high and low frequency were drawn, as shown in Figure 6, using Surfer v18 software. The shape of the artificial delaminations, shown in bold lines, are superimposed with color-coded IE flexural frequency response and corresponding contour lines. The delaminations at 83 mm depth correspond to the high frequency red zones on the contour maps, and the delaminations at 38 mm depth correspond to the low frequency blue zones. This allowed us to conveniently distinguish between the delaminations at different depths. Equation 2 was used in this study as the basis to determine the depth of the delaminations corresponding to the average frequency. The equation represents the theoretical frequency of the fundamental flexural mode of vibration of a thin rectangular plate with simply supported boundary conditions (Mitchell and Hazell 1987).

$$f = \frac{\pi}{2}\left(\frac{1}{a^2}+\frac{1}{b^2}\right)\sqrt{\frac{D}{\rho h}} = \frac{\pi}{2A^2}\left(\frac{P^2}{4} - 2A\right)\sqrt{\frac{D}{\rho h}} = C_{rec}^2\frac{\pi}{2h^2}\sqrt{\frac{D}{\rho h}} \qquad (2)$$

where,

f = Fundamental Frequency for flexural mode of vibration of a simply supported thin rectangle plate
E = Young's Modulus of Elasticity
ρ = Mass Density
h = Depth of Delamination (Plate Thickness)
ϑ = Poisson's Ratio
a, b = Length and Width of Plate
P = Perimeter of Rectangular Plate
A = Planar Area of Rectangular Plate

$$D = \text{Flexural Rigidity} = \frac{Eh^3}{12(1-\vartheta^2)}$$

$$C_{rec}^2 = \frac{h^2}{A^2}\left(\frac{P^2}{4} - 2A\right)$$

Figure 6. *Frequency Contour Maps (1 inch = 25 mm)*

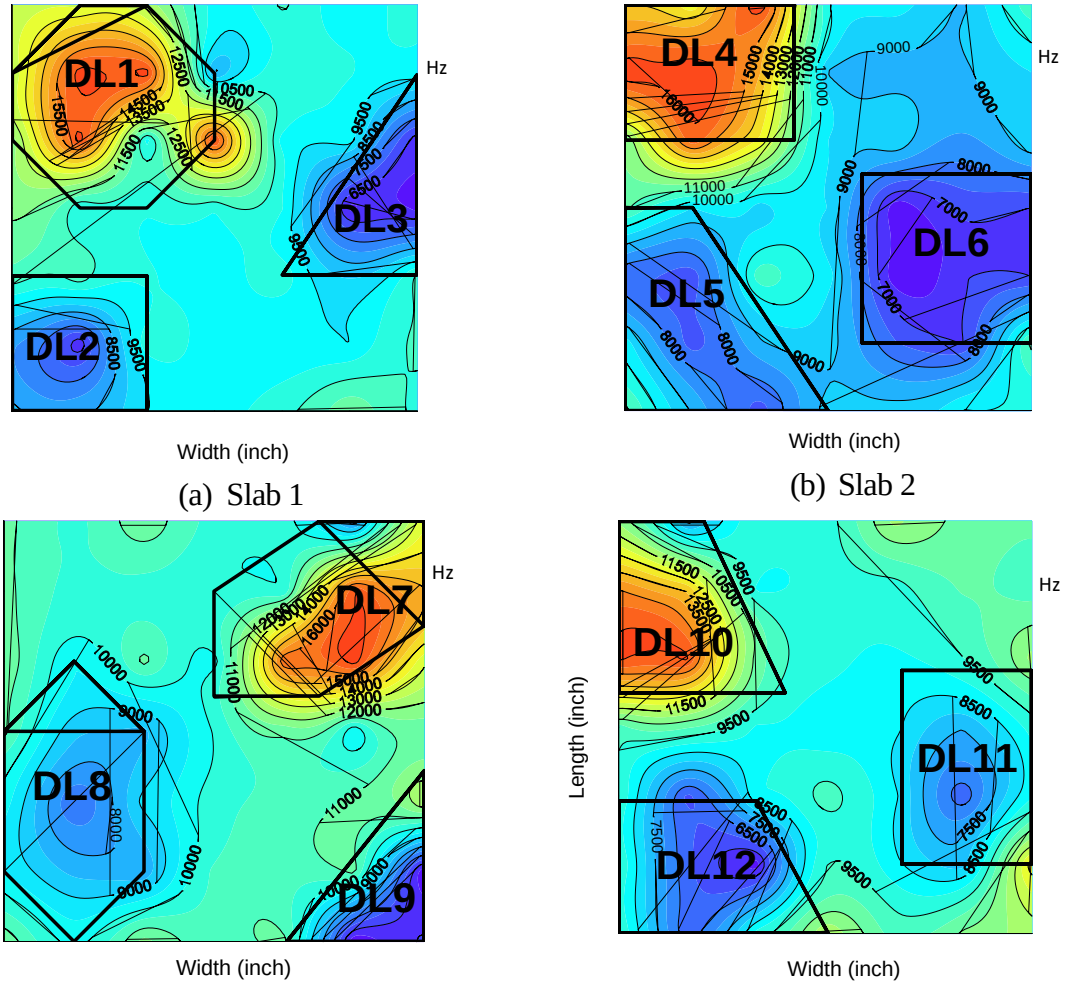

(a) Slab 1 (b) Slab 2

(c) Slab 3 (d) Slab 4

The proposed frequency formulation for our study, based on Equation 2, is presented in Equation 3. The boundary conditions for actual concrete delaminations are in between simply supported and clamped support conditions. To represent the support conditions and the arbitrary shape of delamination, Equation 3 includes a dimensionless frequency term, C_{DL}^2.

$$f_{DL} = C_{DL}^2 \frac{\pi}{2h^2}\sqrt{\frac{D}{\rho h}} = C_{DL}^2 \frac{\pi}{h} \times \frac{C_p}{(1-\vartheta)}\sqrt{\frac{(1-2\vartheta)}{48}} \qquad (3)$$

where,

f_{DL} = Flexural Mode of Frequency for Arbitrarily Shaped Delaminated Plate

C_{DL}^2 = Dimensionless Frequency

$$P - \text{wave velocity}, C_p = \sqrt{\frac{E(1-\vartheta)}{\rho(1+\vartheta)(1-2\vartheta)}} \quad (4)$$

Regression analysis was performed using RStudio software to express the dimensionless frequency in terms of geometric parameters of the delaminations. Three parameters were selected for this purpose (P/h, h/b, Ph/A), as shown in Equations 5, 6 and 7.

$$C_{DL}^2 = \text{func}\left(\frac{P}{h}\right) \quad (5)$$

$$C_{DL}^2 = \text{func}\left(\frac{h}{b}\right) \quad (6)$$

$$C_{DL}^2 = \text{func}\left(\frac{Ph}{A}\right) \quad (7)$$

where,

P = Perimeter of Delaminated Region

A = Area of Delaminated Region

h = Depth of Delamination

$$\frac{1}{\mathrm{b}^2} = \frac{1}{\mathrm{A}^2}\left(\frac{\mathrm{P}^2}{4} - 2\mathrm{A}\right)$$

Graphs were drawn of the dimensionless frequency as a function of the selected parameters. Linear, logarithmic, and exponential functions were fitted. The relationships expressed in Equations 5, 6 and 7 could best be represented by logarithmic and exponential functions. Accordingly, six regression equations were established, as shown in Table 3. All best fit equations yielded *F*-values greater than 1.0 and *P*-values less than 0.05 indicating that these functions are statistically significant. After the regression analysis was completed, the best fit functions for C_{DL}^2were substituted into Equation 3, and the delamination depths were estimated based on the frequencies measured over the delaminations.

The regression functions were established for known delamination geometries and depths, while the depth estimations extend the models to unknown geometries and depths. Table 3 shows that Equation A and B were the most statistically significant with Equation A the best of all with an R^2 value of 0.932. Therefore, these two models, which are based on the delamination parameter P/h were selected for additional assessment. Graphical representations of the actual and estimated concrete delamination depths for these two models are shown in Figure 7. The actual depth is the planned value used in making the specimens. Numerical comparison of the actual and estimated depths, along with the error percentages, are shown in Table 6.

Table 3. *Regression Analysis Results*

Equation No.	Equation from Regression Analysis	Form	R^2	*F*-value	*P*-value
A	$C_{DL}^2 = 3.068 - 0.785 \times \ln\left(\frac{P}{h}\right)$	Logarithmic	0.932	151.7	2.287×10^{-7}
B	$C_{DL}^2 = 2.22e^{-0.060272\left(\frac{P}{h}\right)}$	Exponential	0.883	84.28	3.46×10^{-6}
C	$C_{DL}^2 = 1.308 + 0.574 \times \ln\left(\frac{h}{b}\right)$	Logarithmic	0.434	9.434	0.01181
D	$C_{DL}^2 = 0.106e^{5.19718\left(\frac{h}{b}\right)}$	Exponential	0.465	10.58	0.008677
E	$C_{DL}^2 = 0.783 + 0.691 \times \ln\left(\frac{Ph}{A}\right)$	Logarithmic	0.623	19.21	0.001371
F	$C_{DL}^2 = 0.0816e^{2.293294\left(\frac{Ph}{A}\right)}$	Exponential	0.6847	24.88	0.0005467

Figure 7. *Actual vs. Estimated Delamination Depths*

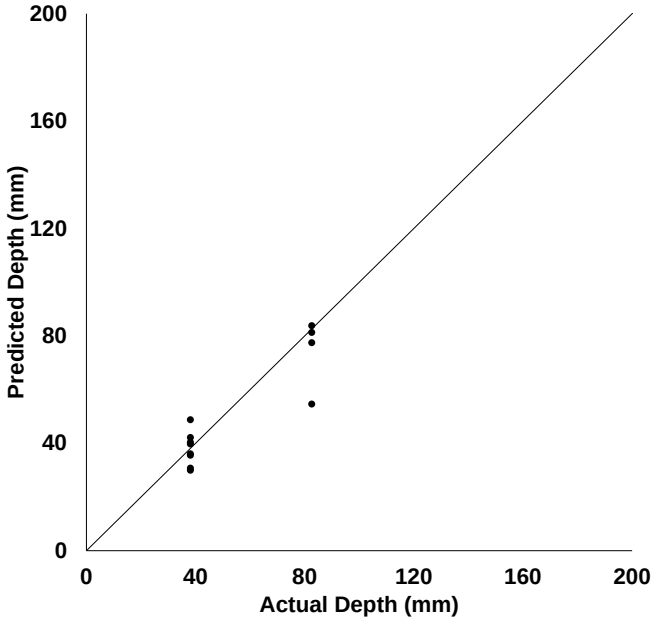

(a) Equation A (Logarithmic)

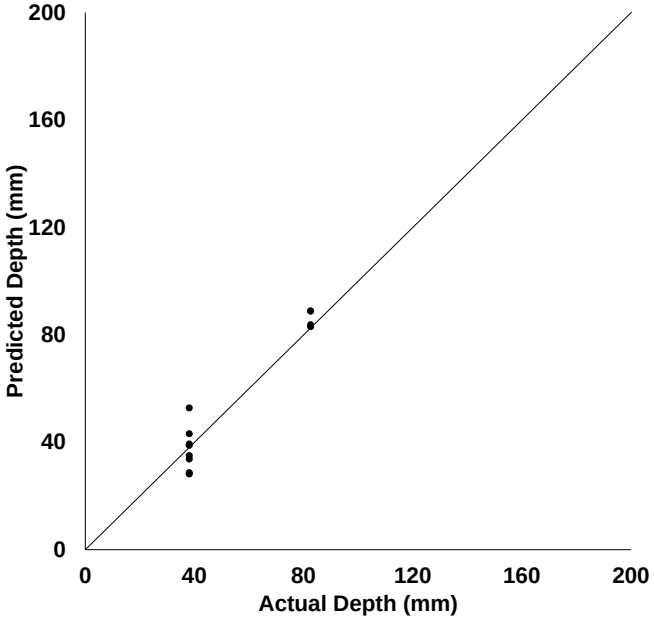

(b) Equation B (Exponential)

Table 4. *Estimated vs. Actual Depths Based on Eq. A and B*

Delamination	Actual Depth (mm)	$f_{DL} = \text{func}\left(\frac{P}{h}\right) \times \frac{\pi}{h} \times \frac{C_p}{(1-\vartheta)}\sqrt{\frac{(1-2\vartheta)}{48}}$			
		Equation A		Equation B	
		Estimated Depth (mm)	Error (%)	Estimated Depth (mm)	Error (%)
DL1	83	81	-1.54	89	7.69
DL2	38	31	-19.27	28	-26.00
DL3	38	36	-6.67	35	-8.00
DL4	83	77	-6.15	84	1.54
DL5	38	49	28.00	53	33.3
DL6	38	40	6.00	39	2.00
DL7	83	84	1.54	89	7.69
DL8	38	42	10.67	43	13.33
DL9	38	30	-21.33	29	-24.67
DL10	83	55	-33.85	83	0.62
DL11	38	40	4.33	39	3.33
DL12	38	36	-5.33	34	-11.33
Average Errors (%)			12		11.6

The actual and estimated values are equal on the solid lines shown in Figure 7. The average errors shown in Table 4 for Equation B and Equation A are practically identical. The percentage of error in the estimated is less than 13%, except for delaminations DL2, DL5, and DL9. Therefore, it may be concluded that both the logarithmic (Equation A) and the exponential (Equation B) correlations of the dimensionless frequency term with perimeter-to-depth ratio are effective in estimating the depth of shallow delaminations of arbitrary shape. The finalized models relating the IE frequency and delamination depth are presented in Equation 7 and 8. Users can consider either of these two models as desired:

$$\text{Measured } f_{DL} = (3.0681853 - 0.7851072 \times \ln\left(\frac{P}{h}\right)) \times \frac{\pi}{h} \times \frac{C_p}{(1-\vartheta)}\sqrt{\frac{(1-2\vartheta)}{48}} \quad (7)$$

$$\text{Measured } f_{DL} = 2.22e^{-0.060272\left(\frac{P}{h}\right)} \times \frac{\pi}{h} \times \frac{C_p}{(1-\vartheta)}\sqrt{\frac{(1-2\vartheta)}{48}} \quad (8)$$

Additional IE data points were collected around the edge of the delaminations for these three delaminations, as shown in Table 5. As a correct IE signal may not be interpreted around the edge due to wave scattering attenuation (Kee and Gucunski 2016), a high percentage of error was observed.

Table 5. *Location of Points where IE Data was Collected*

Delamination	Edge	Internal	Corner
DL1	8	4	8
DL2	8	1	4
DL3	5	1	2
DL4	7	2	2
DL5	7	3	3
DL6	5	4	2
DL7	4	4	1
DL8	8	3	6
DL9	5	1	2
DL10	4	3	1
DL11	4	2	1
DL12	5	2	1

Limitations of the Study

This study has the following limitations:

1. Only two depth levels of delaminations were considered. It is recommended that artificial delaminations be placed at more than two depth levels to further verify the findings of this research.
2. Concrete delaminations in the field will typically have irregular and arbitrary shapes without geometrically sharp corners. Although irregular shaped delaminations were used in this research, they still had sharp corners at the edges which may not fully represent the response of actual delaminations in the field.
3. The proposed models for estimating the depth of arbitrarily shaped delaminations require knowing the perimeter of delamination.

Conclusions and Recommendations

The conclusions drawn from this study, as well as recommendations for future research, are as follows:

- An equation was proposed to estimate the depth of shallow delaminations that is based on the vibration theory of thin rectangular plates with simply supported boundary conditions.
- A dimensionless frequency term was introduced to consider the arbitrary geometry and the semi-clamped boundary conditions of real delamination.
- Tests were conducted on four slabs containing artificial delaminations. The impact-echo test was performed at grid points on the slabs, and the average frequency was determined for each delamination. Regression

analysis was performed to correlate the calculated non dimensional frequency term to the geometry of the delaminations. Six regression functions were proposed, and the functions with the greatest statistical significance were used to relate the frequency of shallow depth delaminations to the depth and P wave speed.

- Both regular-and-irregular-shaped prefabricated delaminations were used in this study which is a unique feature of this research. From the observations it was concluded that the flexural mode frequency measured over a shallow-depth delamination is related to the perimeter-to-depth ratio of the delamination.
- Three parameters, the flexural mode frequency, the P wave velocity, and the perimeter of the delamination, must be known to determine the depth of the shallow depth delamination from Equation 7, or 8. The frequency and the P-wave velocity can be directly obtained from the IE test. In this study, the known perimeter of the artificial delamination was used to estimate the depth. Further research is required to determine the perimeter of the delamination by using the frequency contour map derived from the IE test.
- Due to rough edges and corner points, erroneous results may occur, as they did for DL2, DL5, and DL9. It has been recommended that circular-shaped delaminations, as well as delaminations with curved edges, be used to avoid such errors.
- This study was conducted with 12 delaminations placed in four slab specimens at two depth levels. The number of slab specimens could be increased and the delaminations could be placed at more than two depth levels to obtain a more refined result from the statistical analysis.
- Research to determine whether the response obtained from part of the delamination can be used to predict the depth could be beneficial for interpreting the field data.

Acknowledgments

The authors would like to acknowledge the support of the Department of Civil Engineering of University of Texas at Arlington.

Funding for this project was provided under a grant from the Texas Department of Transportation (TxDOT).

The datasets generated during and/or analysed during the current study are available from the corresponding author on reasonable request.

Mantaka Mahjabin Momo: Sample preparation, NDE scanning, acquisition of data, analysis and interpretation of data and drafting the manuscript. Nur Yazdani: Conceptualization, interpretation of data, manuscript editing, supervision, and funding acquisition. Eyosias Beneberu: Methodology, numerical modelling, test procedure.

References

ASTM (2020) *Standard test method for compressive strength of cylindrical concrete specimens, ASTM C39/C39M-20)*. West Conshohocken, PA: ASTM International.

Carino NJ (2001) The impact-echo method: an overview. In *Structures Congress & Exposition 2001*. Washington, D.C.: American Society of Civil Engineers.

Carino NJ, Sansalone M (1990) Flaw detection in concrete using the impact-echo method. In AS Nowak (ed.), *Proceedings, NATO Conference on Bridge Evaluation, Repair and Rehabilitation*, 101–118. Dordrecht, Netherlands: Kluwer Academic Publishers.

Cheng C, Sansalone M (1993a) The impact-echo response of concrete plates containing delaminations: numerical, experimental, and field studies. *Materials and Structures* 26(159): 274–285.

Gucunski N, Yan M, Wang Z, Fng T, Maher A (2012) Rapid bridge deck condition assessment using three-dimensional visualization of impact echo data. *Journal of Infrastructure Systems* 18(10): 12–24.

Gucunski N, Basily B, Maher A, Kim J, Duong T (2017) Use of robotics in automated and comprehensive NDE of RC structures. In *1st International Conference on Construction Materials for Sustainable Future*, 19-21 April 2017, Zadar, Croatia.

Impact-Echo User's Manual: a self-teaching course and reference for the impact-echo method and software version 2.2a. October 2001.

Kee SH, Gucunski N (2016) Interpretation of flexural vibration modes from impact-echo testing. *Journal of Infrastructure Systems* 22(3): 04016009.

Kee SH, Oh T, Popovics JS, Amdt RW, Zhu J (2012) Nondestructive bridge deck testing with air-coupled impact-echo and infrared thermography. *Journal of Bridge Engineering* 17(6): 928–939.

Lee I, Kwon SH, Park J, Oh T (2017) The effective near-surface defect identification by dynamic behavior associated with both impact-echo and flexural modes for concrete structures. *KSCE Journal of Civil Engineering* 00(0): 1–9.

Mitchell AK, Hazell CR (1987) A simple frequency formula for clamped rectangular plates. *Journal of Sound and Vibration* 118(2): 271–281.

Oh T, Popovics JS, Sim SH (2013b) Analysis of vibration for regions above rectangular delamination defects in solids. *Journal of Sound Vibration* 332(7): 1766–1776.

Olson Instruments, Inc. (2016) *NDE 360 platform with WinIE software version 2.5*. Colorado, USA.

RStudio, r-tools technology.

Sansalone M, Carino NJ (1986) *Impact-echo: a method for flaw detection in concrete using transient stress waves*. Gaithersburg, Maryland: National Bureau of Standards.

Surfer V18, Golden Software, LLC, Colorado, USA.

Zhu J, Popovics JS (2007) Imaging concrete structures using air-coupled impact-echo. *Journal of Engineering Mechanics* 133(6): 628–640.